Comparison of Basis Sets for Efficient *Ab-initio* Modeling of Semiconductors

Dhirendra Vaidya, Saurabh Lodha and Swaroop Ganguly
Department of Electrical Engineering
Indian Institute of Technology Bombay
Mumbai, India, 400076
Email: swaroop.ganguly@gmail.com

***Abstract*—Germanium faces several technological hurdles in replacing silicon and fulfilling its promise as an alternate channel material; namely, low dopant activation, gate stack interface quality, and high contact resistivity for n-Ge. Ab-initio methods could help to address some of these challenges by providing fundamental insight. However, these calculations often tend to be too computationally heavy to be practically useful. In this work, we compare the speed and accuracy of density functional theory (DFT) calculations on the NiGe/Ge Schottky contact using various localized basis sets, and a standard plane wave solver as a complementary DFT solver to affirm on the accuracy. We first compare Atomistix Tool Kit (ATK), a localized-basis DFT solver, to the popular plane wave based Vienna Ab-initio Software Package (VASP) to show that the localized basis sets while being faster, can also match plane wave for accuracy; thereafter, we compare different localized basis sets within ATK.**

I. Introduction

Amongst other technological challenges [1]–[5], higher contact resistance for n-type germanium has been one of the significant hurdles for germanium based CMOS technology. Irrespective of the metal workfunction, large Schottky barrier heights (SBH) are observed in metal/n-Ge contacts on account of Fermi level pinning [6]–[9]. Unlike the phenomenological metal induced gap states (MIGS) theory, the ab-initio methods can account for the interfacial details here. The lower n-SBH observed in epitaxial $NiSi_2$(001)/n-Si(100) contacts [10] had been recently explained using ab-initio methods [11]; this would otherwise be overestimated by MIGS theory [12].

The severe bandgap underestimation of Ge by the local density approximation (LDA) and generalized gradient approximation (GGA) can be overcome by using suitably-calibrated meta generalized gradient approximation (MGGA) functional [13], with little additional computational cost. For MGGA functional within the Atomistix Tool Kit (ATK) [14], Sakata et. al. [15] suggest a localized basis set of $4s, 4p^3, 5s$ and $4d$ orbitals (referred as 'HGH-Tier 4' in Virtual Nanolab [16] from QuantumWise) to get the correct ordering between Γ and L vallies of germanium ($E_{g\Gamma-\Gamma} > E_{g\Gamma-L}$). They calibrate the MGGA functional with a Ge lattice constructed using the experimental lattice constant (5.657 Å). However, we find that if it is constructed using the LDA relaxed lattice constant (5.625 Å) then it is possible to calibrate the MGGA functional to overcome the bandgap underestimation problem with correct bandgap ordering using alternate low-cost basis sets, such as the double zeta polarized (DZP).

Before comparing basis sets, we present the surface study of NiGe (001) using ATK and provide a comparison with a plane wave DFT solver, Vienna abinitio software package (VASP) [17]. This is followed by the computational cost and accuracy studies of different basis sets within ATK. Finally, we present as a case study the SBH calculation performed using different basis sets in ATK. We find that it is possible to calibrate the MGGA functional for Ge using low cost basis set such as DZP which can then reproduce with good accuracy the SBH of NiGe/Ge Schottky contact reported earlier [18]. Such a low cost basis set is useful to simulate the atomic geometries [19], [20] which are more realistic and relevant for device applications but are computationally heavy.

II. Surface study of nickel germanide

We start with the NiGe surface and defects therein, choosing the NiGe (001) surface of MnP-type as in our prior work [18]. We compare the surface energies calculated using ATK and VASP. Surfaces of stoichiometric (0-V) and non-stoichiometric (2Ni-V, 1Ni-V, 2Ge-V, 1Ge-V, Pair-V, Ni-I) NiGe terminations similar to Ref. [21] are studied as a precursor to the NiGe/Ge Schottky barrier study. The stoichiometric NiGe slab is shown in figure 1. Non-stoichiometric slabs are constructed by removing/inserting 1 and/or 2 Ge and/or Ni atoms from/near the surface. We first study the stoichiometric NiGe surface reconstruction in terms of the rumpling factor, which is shown in Table I. It is seen to be qualitatively similar to that obtained from VASP GGA calculations [21]. Next we calculate the surface energy of NiGe for stoichiometric and non-stoichiometric configurations, using a thermodynamic formulation [21]. The surface energy is given as $E_{surface} = (1/2)(E_{slab} - N_{Ge}E_{Ge} - N_{Ni}E_{Ni} + N_{Ge}(2\Delta H_f) + (N_{Ge} - N_{Ni})\mu_{Ni})$. Where, E_{slab} is the total energy of the simulated slab, $E_{Ge}(E_{Ni})$ is the energy per atom of bulk Ge(Ni). $N_{Ge}(N_{Ni})$ is the number of atoms in bulk Ge(Ni). μ_{Ni} is the chemical potential of nickel. $(-2\Delta H_f)$ is the formation energy of NiGe. Relating the surface energy to the chemical potential of Nickel elucidates the surface formation under nickel-rich and nickel-poor conditions. $\mu_{Ni} = 0$ corresponds to the nickel rich condition, whereas $\mu_{Ni} = -2\Delta H_f$ is the germanium rich (nickel poor)

© 2017 The Japan Society of Applied Physics

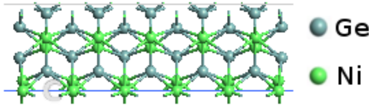

Fig. 1. Simulated surface slab of stoichiometric (0-V) NiGe (001)

TABLE I
COMPARISON OF RUMPLING FACTOR OF NiGe (001) SURFACE

	$\delta r_1(\%)$	$\delta r_2(\%)$	$\delta r_3(\%)$	$\delta r_4(\%)$
VASP-GGA [21]	-9.8	2.0	-2.9	0.7
ATK-LDA	-11.68	3.37	-4	1.11

condition. It can be seen from figure 2 that, except for the 2Ge-V, the surface energies for the other configurations from ATK are in agreement with those from VASP. Different geometry relaxation algorithms (Limited-memory Broyden-Fletcher-Goldfarb-Shanno (L-BFGS) in ATK and conjugate gradient in VASP) which result in different surface reconstruction could be the cause of disagreement for the 2Ge-V configuration.

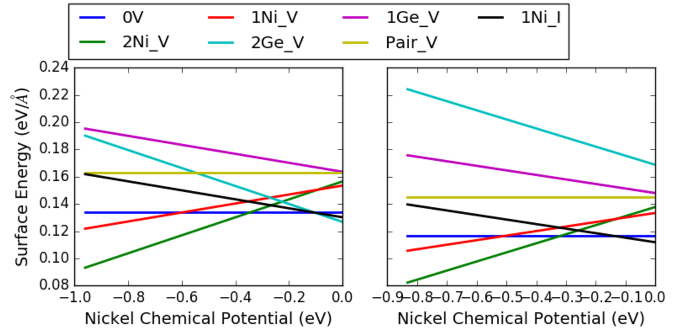

Fig. 2. Comparison of surface energy calculations of ATK (left) and VASP (right). The calculations agree except for 2Ge-V. In Ni rich conditions, 0-V NiGe (001) has lowest surface energy, whereas in Ge rich conditions 2Ni-V is the lowest energy surface.

III. CALIBRATION OF MGGA FUNCTIONAL AND CONFINEMENT EFFECTS IN Ge

We find that the MGGA functional can be calibrated using HGH-Tier 4 basis [18], double zeta double polarized (DZDP) basis and more importantly using a computationally efficient localized basis such as double zeta polarized (DZP) basis at LDA relaxed lattice constant $a_{Ge} = 5.625$ Å to produce correct ordering between L and Γ and Δ valley gaps ($E_{g\Gamma-\Delta} > E_{g\Gamma-\Gamma} > E_{g\Gamma-L}$). Figure 3 shows the calibration of the 'c' parameter of the MGGA functional for three different localized basis sets: DZP, DZDP and the HGH-Tier 4 (used in [18]). It can be seen that all three basis sets correctly produce an indirect $\Gamma - L$ bandgap ≈ 0.67 eV. Table II lists the bandgap values as well as effective masses calculated using the MGGA functional calibrated at the LDA relaxed lattice constant. All three basis sets produce accurate longitudinal and transverse effective masses. In terms of calculation speed (Table II), we find that the DZP basis takes about half the time compared to DZDP and HGH-Tier 4 while giving results that are close; this makes it a very attractive basis set for larger slab geometries. We also test this efficient localized basis by studying bandgap widening (figure 4) due to quantum confinement in Ge (100) slabs. Along with inverse square relation with the slab thickness, the bandgap widening in the conduction band is inversely proportional to the effective masses (m_l and m_t), however the bandgap widening in the valence band is more complex because of the warped nature of the valence bandstructure. However we find that the overall bandgap widening can be effectively captured in a quantization effective mass which can be calculated by fitting a parabola to the bandgap at various slab thicknesses. The calculated quantization effective mass is seen to agree

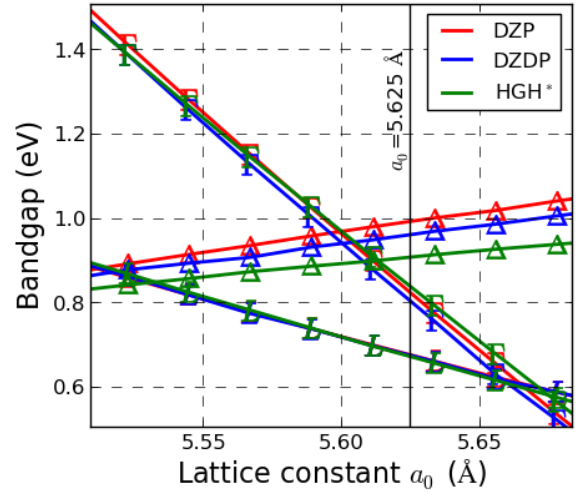

Fig. 3. Calibration of MGGA functional for different basis sets. Calibrated 'c' parameter for DZP, DZDP and HGH-Tier 4 is 0.99, 0.99 and 0.94 respectively. *Vaidya et. al. [18]

with the previously reported value [18] as well as with VASP GGA+U calculations.

IV. NiGe/Ge SCHOTTKY BARRIER STUDY

For a device-oriented case study for the DZP basis, we calculated the Schottky barrier height (SBH) at the NiGe (001)/Ge (100) interface and compared it with the SBH calculated using DZDP and HGH-Tier 4 in Ref. [18]. The SBH may be calculated using the band alignment (BAM) method or density-of-states (DOS) method. Using the DZP basis and DZDP basis, we calculated the p-SBH to be 0.23 eV, reasonably close to our previously reported value of 0.26 eV in Ref. [18]. Figure 5 shows the macroscopic average of electron difference density near the interface illustrating the formation of a dipole at the interface. Calculations based on DZP and HGH-Tier 4 are seen to agree exactly. They are also consistent with each other when the p-SBH is extracted from the DOS method (Table III, figure 6). Figure 6 shows the DOS projected on to the p-orbitals of Ge atom at ≈ 31 Å away from

TABLE II
CALIBRATION OF MGGA FUNCTIONAL AND CALCULATED BANDSTRUCTURE PARAMETERS

	c	$E_{g\Gamma-L}$ (eV)	$E_{g\Gamma-\Gamma}$ (eV)	$E_{g\Gamma-\Delta}$ (eV)	m_l	m_t	m_Γ	Diagonalization time per step (in sec)	
								2 Ge atoms	40 Ge atoms
DZP	0.99	0.67	0.82	0.99	1.53	0.09	0.039	2.03	91.76
DZDP	0.99	0.67	0.8	0.96	1.63	0.09	0.039	2.04	221.02
HGH-Tier 4 [18]	0.94	0.67	0.84	0.91	1.53	0.09	0.039	2.53	170.43
VASP-GGA+U	–	0.74 [22]	0.89 [22]	0.92 [22]	–	–	0.06 [22] 0.046 [23]	–	–
Expt [24]	–	0.66	0.8	0.85	1.59	0.08	0.042	–	–

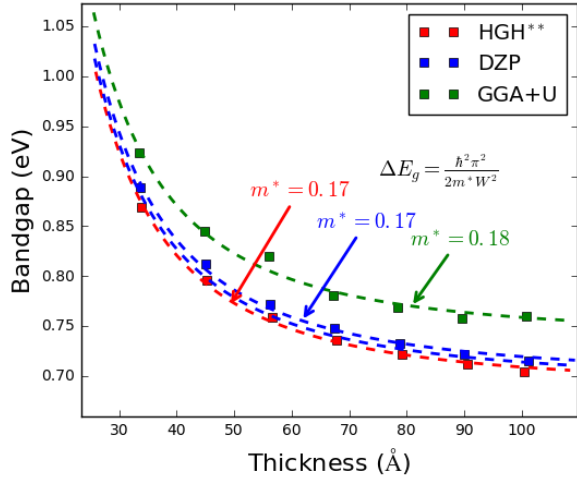

Fig. 4. Bandgap widening due to confinement of Ge(100). The quantization effective masses calculated using DZP basis in ATK, HGH-Tier 4 basis in ATK and GGA+U in VASP agree well.
**Vaidya et. al. [18]

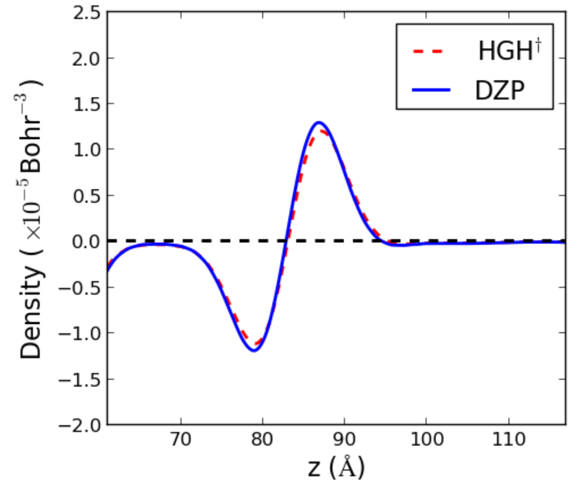

Fig. 5. Dipole formation at the NiGe/Ge interface. It can be seen that DZP and HGH-Tier 4 produce very similar dipoles at the interface.
†Vaidya et. al. [18]

TABLE III
COMPARISON OF DIFFERENT LOCALIZED BASIS IN THE CALCULATION OF NiGe/Ge p-SBH.

	0-V (BAM) (eV)	0-V (DOS) (eV)	1Ni-V(BAM) (eV)	1Ni-V(DOS) (eV)
DZP	0.23	0.24	0.01	0.0
DZDP	0.23	0.25	–	
HGH-Tier 4 [18]	0.26	0.28	0.02	0.03

the NiGe/Ge interface. To further assess the performance of the DZP basis, we simulated the 1Ni-V configuration reported in [18], which is shown to give the lowest p-SBH. The calculated value of the p-SBH for 1Ni-V is 0.01 eV, which also agrees well with the value reported there.

V. CONCLUSION

In summary, we provide a calibration of the MGGA functional with ATK's computationally efficient preset basis sets to correctly produce Ge bandstructure. A comparison of ATK and VASP demonstrates that localized basis DFT on Ge can be a computationally efficient choice with no compromise on accuracy. A case study of the NiGe/Ge Schottky contact using calibrated MGGA functional in ATK with the efficient localized basis set DZP shows no deviation from the previous conclusion drawn using the more costly basis set HGH-Tier 4. Thus the DZP localized basis may be recommended as a speedy and accurate option for realistic, device-oriented materials modeling.

APPENDIX
COMPUTATIONAL METHODOLOGY

In this paper we use DFT solvers from ATK (localized basis) as well as VASP (plane wave). For slab simulations using ATK, we have sampled the Brillouin zone using 9x9x1 Monkhorst-Pack grid and density mesh cutoff of 75 Hartree for relaxation of NiGe surface slab as well as the relaxation of NiGe/Ge interfaces. For the Schottky barrier height extractions we used 18x18x1 Monkhorst-Pack grid for Brillouin zone sampling and density mesh cutoff of 110 Hartree. Tolerance

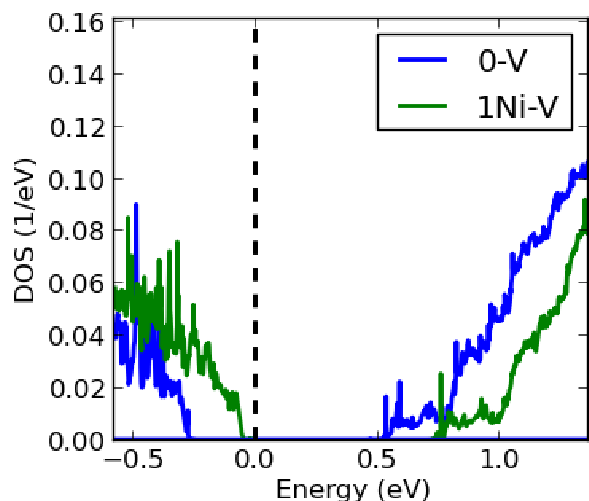

Fig. 6. DOS projected onto p-orbitals of Ge atom ≈ 31 Åaway from the NiGe/Ge interface for 0-V and 1Ni-V configuration.

of 10^{-4} Hartree is used and forces were minimized to 0.01 eV/Å. LDA functional with Perdew-Zunger parameterization [25] is used for relaxation whereas MGGA functional is used in simulations NiGe/Ge interface slab geometry for the SBH calculation. For Ge slab simulations for the confinement effect study, Monkhorst-Pack grid of 21x21x1 and density mesh cutoff of 110 Hartree was used. Ge slabs are constructed with LDA relaxed lattice constant of $a_{Ge} = 5.625$ Å. In all the slab geoetries, the periodic images are separated by sufficiently large vacuum region.

VASP is used as a plane wave DFT solver for NiGe surface energy calculations with pseudopotentials generated using projected augmented wave method [26], [27]. The surface energies are compared with ATK-DFT results. For VASP we use Brillouin zone sampling of 4x4x1 and energy cutoff of 380 eV is used. The NiGe surface slab is relaxed using LDA functional with Perdew-Zunger [25] parameterization. In the Ge bandgap widening calculations, GGA+U (U=0 eV, J=3.33 eV) approach is used with cut off energy of 312.5 eV and Monkhorst-Pack grid of 16x16x1 (25x25x1 for DOS calculations) is used. GGA+U method gives the lattice constant of 5.59 Å. All the simulated slabs for confinement study were constructed using GGA+U relaxed lattice constant.

References

[1] D. Kuzum, T. Krishnamohan, A. Nainani, Y. Sun, P. A. Pianetta, H. S. P. Wong, and K. C. Saraswat, "High-mobility Ge N-MOSFETs and mobility degradation mechanisms," *IEEE Trans. Electron Devices*, vol. 58, no. 1, pp. 59–66, Jan 2011.

[2] C. O. Chui, K. Gopalakrishnan, P. B. Griffin, J. D. Plummer, and K. C. Saraswat, "Activation and diffusion studies of ion-implanted p and n dopants in germanium," *Appl. Phys. Lett.*, vol. 83, no. 16, pp. 3275–3277, 2003.

[3] S. V. Elshocht, M. Caymax, T. Conard, S. D. Gendt, I. Hoflijk, M. Houssa, B. D. Jaeger, J. V. Steenbergen, M. Heyns, and M. Meuris, "Effect of hafnium germanate formation on the interface of HfO_2/germanium metal oxide semiconductor devices," *Appl. Phys. Lett.*, vol. 88, no. 14, p. 141904, 2006.

[4] S. Kothari, C. Joishi, S. Ghosh, D. Biswas, D. Vaidya, S. Ganguly, and S. Lodha, "Improved n-channel ge gate stack performance using HfAlO high-k dielectric for various Al concentrations," *Appl. Phys. Exp.*, vol. 9, no. 7, p. 071302, 2016.

[5] S. Kothari, C. Joishi, H. Nejad, N. Variam, and S. Lodha, "Plasma-assisted low energy N_2 implant for V_{fb} tuning of Ge gate stacks," *Appl. Phys. Lett.*, vol. 109, no. 7, p. 072105, 2016.

[6] A. Dimoulas, P. Tsipas, A. Sotiropoulos, and E. Evangelou, "Fermi-level pinning and charge neutrality level in germanium," *Appl. Phys. Lett.*, vol. 89, no. 25, pp. 252 110–252 110, 2006.

[7] T. Nishimura, K. Kita, and A. Toriumi, "Evidence for strong fermi-level pinning due to metal-induced gap states at metal/germanium interface," *Appl. Phys. Lett.*, vol. 91, no. 12, 2007.

[8] R. K. Mishra, U. Ganguly, S. Ganguly, S. Lodha, A. Nainani, and M. C. Abraham, "Nickel germanide with rare earth interlayers for Ge CMOS applications," in *Electron Devices and Solid-State Circuits (EDSSC), 2013 IEEE International Conference of*, June 2013, pp. 1–2.

[9] Y. Tong, B. Liu, P. S. Y. Lim, and Y. C. Yeo, "Selenium segregation for effective schottky barrier height reduction in NiGe/n-Ge contacts," *IEEE Electron Device Lett.*, vol. 33, no. 6, pp. 773–775, June 2012.

[10] R. T. Tung, A. F. J. Levi, J. P. Sullivan, and F. Schrey, "Schottky-barrier inhomogeneity at epitaxial $NiSi_2$ interfaces on Si(100)," *Phys. Rev. Lett.*, vol. 66, pp. 72–75, Jan 1991.

[11] J. Kim, B. Lee, Y. Park, K. V. R. M. Murali, and F. Benistant, "Ab-initio study on schottky-barrier modulation in $NiSi_2$/Si interface," in *2015 International Conference on Simulation of Semiconductor Processes and Devices (SISPAD)*, Sept 2015, pp. 226–229.

[12] R. T. Tung, "The physics and chemistry of the schottky barrier height," *Appl. Phys. Rev.*, vol. 1, no. 1, p. 011304, 2014.

[13] F. Tran and P. Blaha, "Accurate band gaps of semiconductors and insulators with a semilocal exchange-correlation potential," *Phys. Rev. Lett.*, vol. 102, p. 226401, Jun 2009.

[14] Atomistix Toolkit version 2015.1, Quantumwise A/S. (www.quantumwise.com).

[15] K. Sakata, B. Magyari-Köpe, S. Gupta, Y. Nishi, A. Blom, and P. Deák, "The effects of uniaxial and biaxial strain on the electronic structure of germanium," *Comput. Mater. Sci.*, vol. 112, Part A, pp. 263 – 268, 2016.

[16] Virtual nanolab version 2015.1, Quantumwise A/S. (www.quantumwise.com).

[17] G. Kresse and J. Furthmüller, "Efficient iterative schemes for ab initio total-energy calculations using a plane-wave basis set," *Phys. Rev. B*, vol. 54, pp. 11 169–11 186, Oct 1996.

[18] D. Vaidya, S. Lodha, and S. Ganguly, "Ab-initio study of NiGe/Ge schottky contact," *J. Appl. Phys.*, vol. 121, no. 14, p. 145701, 2017.

[19] D. Stradi, U. Martinez, A. Blom, M. Brandbyge, and K. Stokbro, "General atomistic approach for modeling metal-semiconductor interfaces using density functional theory and nonequilibrium green's function," *Phys. Rev. B*, vol. 93, p. 155302, Apr 2016.

[20] A. Blom, U. M. Pozzoni, T. Markussen, and K. Stokbro, "First-principles simulations of nanoscale transistors," in *2015 International Conference on Simulation of Semiconductor Processes and Devices (SISPAD)*, Sept 2015, pp. 52–55.

[21] M. K. Niranjan, L. Kleinman, and A. A. Demkov, "Electronic structure, elastic properties, surface energies, and work functions of NiGe and PtGe within the framework of density-functional theory for various surface terminations," *Phys. Rev. B*, vol. 75, p. 085326, Feb 2007.

[22] H. Tahini, A. Chroneos, R. W. Grimes, U. Schwingenschlögl, and H. Bracht, "Diffusion of e centers in germanium predicted using GGA+U approach," *Appl. Phys. Lett.*, vol. 99, no. 7, 2011.

[23] S. Gupta, R. Chen, B. Magyari-Kope, H. Lin, B. Yang, A. Nainani, Y. Nishi, J. S. Harris, and K. C. Saraswat, "Gesn technology: Extending the ge electronics roadmap," in *2011 International Electron Devices Meeting*, Dec 2011, pp. 16.6.1–16.6.4.

[24] http://www.ioffe.ru/SVA/NSM/Semicond/Ge/bandstr.html.

[25] J. P. Perdew and A. Zunger, "Self-interaction correction to density-functional approximations for many-electron systems," *Phys. Rev. B*, vol. 23, pp. 5048–5079, May 1981.

[26] P. E. Blöchl, "Projector augmented-wave method," *Phys. Rev. B*, vol. 50, pp. 17 953–17 979, Dec 1994.

[27] G. Kresse and D. Joubert, "From ultrasoft pseudopotentials to the projector augmented-wave method," *Phys. Rev. B*, vol. 59, pp. 1758–1775, Jan 1999.